Calculations and analysis of ⁵⁵Mn nuclear quadrupole coupling for asymmetric top acyl methyl manganese pentacarbonyl

Chakree Tanjaroon,^a David D. Mills,^b Carlos A. Jiménez Hoyos^c, and Stephen G. Kukolich^b

^aDepartment of Chemistry and Biochemistry, James Madison University, Harrisonburg, Virginia 22807,

^bDepartment of Chemistry and Biochemistry, University of Arizona, Tucson, AZ 85721 ^cDepartment of Chemistry. Wesleyan University, Middletown, CT 06459

(abstract)

Revised assignments of the measured transitions for the asymmetric top acyl isomers of methyl manganese pentacarbonyl are presented, along with a corresponding fit to determine rotational and quadrutpole coupling constants. New assignments for measured transitions give a better fit to the spectrum and better agreement between experimental and calculated quadrupole coupling strengths. The best agreements were obtained for B3LYP and M11 DFT calculations with triple and quadruple-zeta basis sets. Experimental molecular parameters from the new analysis are: A = 840.0843(52), B = 774.2861(17), C = 625.6528(13). D_J = 0.000212(21). D_{JK} = 0.00488(18), $1.5\chi_{aa}$ = -46.96(11), $0.25(\chi_{bb} - \chi_{cc})$ = -13.44(3) MHz.

I. Introduction

The importance of alkyl group migration and carbonyl insertion in catalytic reactions is widely recognized in organometallic chemistry. One of the fundamental migration-insertion reactions is the thermal carbonylation and photodecarbonylation of the methyl manganese pentacarbonyl complex. In the thermal carbonylation and photodecarbonylation of CH₃Mn(CO)₅ experiments[1], Calderzarro and Cotton speculated that methyl migration was a key step in this reaction. Noack and Calderzarro[2] found the by product *cis*-CH₃C(O)Mn(CO)₄ which supported this analysis. Results of IR spectroscopy measurements [3] and other kinetic experiments suggested that acyl-Mn isomers are important in methyl migration and carbonyl insertion reactions of CH₃Mn(CO)₅.

Quantum chemical calculations by Maynick, et al[4] obtained three, low energy stable structures of methylmanganese pentacarbonyl. They proposed that possible isomerization of the reactant CH₃Mn(CO)₅ could form the asymmetric acyl-Mn isomer as an important step in the carbonalization reaction. The isomerization reaction shown in equation 1 below involves the methyl migration and the agostic stabilized transition states in the pathway.

 $CH_3Mn(CO)_5 \rightarrow agostic stabilized transition states \rightarrow CH_3C(O)Mn(CO)_4$ (1)

Some recent density functional theory calculations found two stable isomeric structures for the acyl-Mn isomers of CH₃C(O)Mn(CO)₄. The optimized molecular geometries of the two stable acyl-Mn isomers are depicted in Figure 1. The lowest energy isomer (1a) is the symmetric CH₃Mn(CO)₅ and the two distinct acyl-Mn isomers are the agostic form (1b) and the dihapto form(1c).

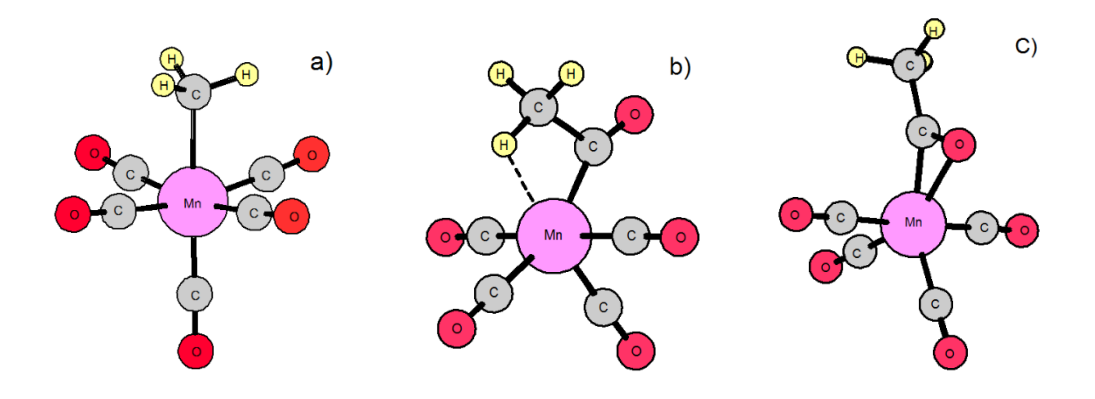


Figure 1. The three isomeric structures of methyl manganese pentacarbonyl. Structure 1a, the symmetric top structure has the lowest energy. (1b) is the agostic form and (1c) is the dihapto form.

Microwave spectroscopy measurements combined with theoretical calculations can identify which of the possible structural isomers are present in the gas phase. The rotational constants A, B, and C ae directly obtained with high accuracy from the measurements and reliable values are also obtained from the calculations. The two acy structures (1b and1b) are asymmetric tops and show distinct microwave spectra. The ⁵⁵Mn quadrupole coupling interaction causes easily resolvable splittings in the spectrum and the splitting patterns further help to identify which isomer is observed.

Rotational transitions for the asymmetric top acyl methyl manganese pentacarbonyl complex, CH₃(CO)Mn(CO)₄, were measured[5] with high accuracy using a Flygare-Balle type microwave spectrometer.[6] These measurements provide the rotational constants and ⁵⁵Mn quadrupole coupling interaction strengths. Previous measurements[5] showed that the structure of acyl methyl manganese pentacarbonyl in the gas phase, liberated from solvent molecules, is most consistent with the predicted dihapto structure of Figure 1b. In that preliminary work, the ⁵⁵Mn quadrupole strengths for CH₃(CO)Mn(CO)₄ were determined by fitting the quadrupole hyperfine splitting patterns. However, there was serious disagreement between the calculations and the microwave experiment (and among calculations themselves) regarding the magnitude and the sign of the quadrupole coupling strengths for CH₃(CO)Mn(CO)₄. The present work focuses on resolving this disagreement between theory and experiment.

The present work reports on the reanalysis of the spectrum of the asymmetric top acyl methyl manganese pentacarbonyl complex. This work is guided by new calculations to reevaluate the nuclear quadrupole coupling constants, the previous work on the asymmetric top acyl methyl manganese[5] revealed reasonably good agreement between the experimental and theoretical rotational constants, but the quadrupole coupling strengths varied significantly between methods and showed poor agreement with experimentally determined nuclear quadrupole coupling constants. To rectify the poor agreement between theory and experiment, new computations were run, some with uncontracted basis sets for Mn. The results presented here show that the DFT method worked quite well in this case to compute the nuclear quadrupole coupling strengths to reasonably high accuracy.

II. Spectral Analysis

The observed spectrum is congested due to asymmetry and hyperfine splittings. There is the possibility that both the dihapto and agostic forms contribute to some regions of the spectrum. Additional splittings caused by the methyl internal rotation are possible for the dihapto asymmetric molecule depending on the methyl torsional barrier height. In total, 172 lines were observed between 4 to 8 GHz region; about half of these lines were considered rather weak based on the number of times the frequency could be measured above and below the peak frequency. 40 hyperfine components of the four R-branch lines, $J = 2 \rightarrow 3$, $3 \rightarrow 4$, $4 \rightarrow 5$, and $5 \rightarrow 6$, were assigned to CH₃(CO)Mn(CO)₄. Quantum number assignment was made possible by carefully matching the experimental spectrum to the simulated spectrum with initial parameters obtained from ab initio calculations. The spectrum was fit using a rigid rotor Hamiltonian. We performed least-squares fit with Watson S-reduced prolate Hamiltonian using the JPL Pickett's SPFIT/SPCAT program[7]. This 7-parameters fit included the rotational constants A, B, and C, the centrifugal distortion constants D_J and D_{JK}, and the quadrupole parameters $1.5\chi_{aa}$ and $0.25(\chi_{bb} - \chi_{cc})$. where χ is used to denote the quadrupole coupling strength, eQq, where e is the electron charge, Q is the electric quadrupole moment of ⁵⁵Mn, and q is the electric field gradient along the inertial axis, a,

b and *c*. In the units of MHz, $\chi(\text{MHz}) = 234.9647 \times \text{Q(barn)} \times \text{q(a.u.)}[8]$. The nuclear quadrupole moment of ⁵⁵Mn atom is relatively large (330 mb)[9]. Therefore, we expect strong coupling with the electric field gradient about the nucleus and relatively large eQq value in this complex. The fit results, root mean square error, and 1σ standard error (67% confidence level) are given in Table 1. Table 2 shows observed frequencies and calculated frequencies computed from the best least-squares fit for the dihapto isomer. Quantum number assignments were assigned according to F = J + I angular momentum coupling scheme (F is round up to whole number). The pseudo quantum number $K_a K_c$ is used to label asymmetry splitting. We note in Table 1, that the rotational constants have not changed significantly with the new fit but the quadrupole coupling values are substantially different and now in much better agreement with calculated values.

Table 1. Rotational constants, centrifugal distortion constants, and the nuclear quadrupole hyperfine coupling constants obtained from the best least-squares fit. Spectroscopic constants are in MHz. 1σ standard error = 18 kHz for the fit.

Experimental constant	This work	Previous work[Error!		
		Bookmark not defined.]		
A	840.0843(52)	839.955(42)		
В	774.2861(17)	774.203(67)		
С	625.6528(13)	625.628(14)		
DJ	0.000212(21)	-		
D _{JK}	0.00488(18)	-		
1.5χ _{aa}	-46.96(11)	44.9(47)		
0.25(χ _{bb} - χ _{cc})	-13.44(3)	11.9(12)		
Number of lines	40	31		
RMS, kHz	16	39		
1σ, kHz	3	41		

Table 2. Observed and calculated fit frequencies (MHz).

Јкакс→	J' _{Ka'Kc'}	F→	F'	Observed	Calculated	Obs. – Calc.	
3 ₃₁	2 ₂₁	1	1	4948.9594	4948.9646	-0.00516	
4 ₁₃	3 ₁₂	5	6	5570.2344	5570.2270	0.00736	
4 ₁₃	312	6	6	5570.5930	5570.5842	0.00881	
4 ₁₃	312	5	5	5570.8934	5570.8713	0.02213	
4 ¹³	312	5	4	5570.8934	5570.8794	0.01400	
4 ₁₃	312	6	5	5571.2264	5571.2284	-0.00202	
431	3 ₂₁	5	4	6371.0428	6371.0527	-0.00987	
431	3 ₂₁	5	5	6371.0428	6371.0521	-0.00931	
4 ₁₃	303	4	3	6411.9379	6411.9427	0.00476	
4 ₁₃	3 ₀₃	3	3	6413.7332	6413.7295	0.00372	
423	3 ₁₃	3	3	6432.5583	6432.5556	0.00275	
5 ₁₅	4 ₁₄	6	6	6432.8545	6432.8589	-0.00445	
423	313	5	5	6432.9602	6432.9919	-0.03174	
4 ₂₃	3 ₁₃	5	4	6433.0220	6432.9943	0.02769	
5 05	404	6	6	6433.2539	6433.2336	0.02031	
423	3 ₁₃	6	5	6433.3471	6433.3404	0.00671	
5 15	414	5	4	6433.5597	6433.5583	0.00137	
5 15	414	4	3	6433.6426	6433.6782	-0.03562	
5 ₀₅	4 ₀₄	5	4	6433.9471	6433.9326	0.01447	
5 05	404	4	3	6434.0541	6434.0518	0.00231	
4 ₂₃	3 ₁₃	4	5	6434.1097	6434.1074	0.00233	
423	3 ₁₃	4	4	6434.1097	6434.1097	-0.00003	
5 ₀₅	4 ₀₄	6	5	6434.5340	6434.5182	0.01577	
5 15	414	3	2	6434.6960	6434.7363	-0.04027	
5 15	414	7	6	6435.0143	6434.9955	0.01877	
5 05	404	3	2	6435.0928	6435.1091	-0.01634	

5 05	4 ₀₄	7	6	6435.3732	6435.3702	0.00301
5 15	414	8	7	6435.4603	6435.4700	-0.00966
4 ₄₁	3 ₃₁	7	6	6614.9449	6614.9794	-0.03453
4 ₄₁	3 ₃₁	6	5	6615.5978	6615.5763	0.02153
4 ₄₁	3 ₃₁	2	1	6615.7941	6615.7832	0.01089
616	5 ₁₅	7	6	7685.6269	7685.6524	-0.02554
616	5 ₁₅	4	3	7686.0249	7686.0160	0.00890
606	505	4	3	7686.0696	7686.0643	0.00529
616	5 15	8	7	7686.2674	7686.2601	0.00730
606	505	8	7	7686.3208	7686.3085	0.01229
616	515	9	8	7686.5690	7686.5723	-0.00334
606	505	9	8	7686.6211	7686.6207	0.00043
616	515	6	7	7686.6878	7686.6854	0.00238
606	5 ₀₅	6	7	7686.7366	7686.7338	0.00277

III. Computational

High-level Gaussian (G16) calculations were done at Wesleyan University and the University of Arizona. The calculations at Arizona were done on the ocelote HPC, 28 processor system using 268 Gb memory[10]. The primary software used in all calculations was the Gaussian-16 suites (G-16)[11]. The use of the keyword "output=pickett" provides microwave parameters, such as A, B and C, as well as the electric field gradients (EFG), which lead directly to the ⁵⁵Mn quadrupole coupling values at the Mn-atoms in the IA (inertial axis) axis system. Initial optimizations were performed beginning from the optimized M11/aug-cc-pVTZ structures from previous work[5] using varying methods with a Def2TZVPP basis set. For some calculations, the geometry optimization was followed by single point computations at a higher level with fixed geometry to obtain better EFG values. These calculations involved a split basis set (Def2QZVPP for Mn and Def2TZVPP for the other elements).

The results of the newer calculations for asymmetric top acyl methyl manganese are shown in Table 3 (at end). The experimental parameters which provided the best fit to the assigned experimental lines, using spfit, are in the first column. The DFT results in columns 3, 4 and 5 yielded rotational constants within 2% of experimental values. The ab-initio MP2 rotational constants are not as good, which may be the result of MP2 calculations predicting excessive ionic character in the Mn-Me bond, giving a very short bond distance. The 1.5 χ_{aa} values are within 2% across the first 5 columns (dihapto). Wider variations were seen for some of the other functionals tested. The variations of the 0.25(χ_{bb} - χ_{cc}) terms are significantly larger, up to 7 MHz. The MP2 result was closer, within 1.5 MHz.

The nuclear quadrupole coupling constants displayed in table 3 show a good agreement between different methods for the same structure. This offers increased optimism that computational and experimental nuclear quadrupole coupling constants can be used to determine the preferred isomer of the asymmetric top acyl methyl. We note that calculated parameters for the agostic isomer are much different from experimental values. The good agreement of nuclear quadrupole coupling constants between different methods, along with the stark difference in calculated $1.5\chi_{aa}$ values, strongly suggests the lower energy asymmetric form of methyl manganese pentacarbonyl is the dihapto form. In addition, as was also observed in our previous work¹, the calculated rotational constants for the dihapto form show much better agreement with the experimental rotational constants, as compared to the calculated rotational constants for the agostic form.

Table 3. The experimental and calculated molecular parameters for dihapto (+3 agostic) isomers of CH₃Mn(CO)₅ in MHz. Basis sets used for optimizations are provided below. Optimizations which were followed by single-point EFG calculations were performed as noted in the text. For the experimental results, 40 transitions were included with rms = 16 kHz and a standard deviation of 18 kHz for the experimental fit.

Parameter	1. Experimental	2.B3LYP –dihapto	3. M11- dihapto	4. CCSD - dihapto	5. MP2 - dihapto	6. B3LYP- Agos	7. PBE1PBE- Agos
А	840.0843(52)	825.589	831.458	833.095	938.300	819.810	840.899
В	774.2861(17)	770.664	778.362	777.454	838.050	788.101	807.776
С	625.6528(13)	635.694	637.850	641.665	706.278	654.867	669.182
1.5 χ aa	-46.96(11)	-46.5	-45.50	-40.65	-47.3	-97.1	-94.6
0.25(χ _{bb} - χ _{cc})	-13.44(3)	-7.2	-6.667	-7.69714	-11.9	-12.9	-13.2
Mu-a		2.65	2.14	2.125	5.39	-1.01	-0.98
Mu-c		-0.62	0.87	0.590	0.68	-2.93	-2.97
X _{aa}		-31.0		-27.10	-31.5	-64.7	-63.1
X bb		1.1		-1.85	-8.0	6.6	5.1
X cc		29.9		28.94	39.5	58.1	57.9
Method/ Basis set		B3LYP/D ef2TZVP P	M11/def2 QZVPP	CCSD/cc- pVQZ,	MP2/Def 2TZVPP	B3LYP/De f2TZVPP	PB1PBE/Def 2TZVPP
Single Point EFG Calculation (Y/N)		Υ	N	N	Υ	Υ	Y

IV. Results and Discussion

New experimental values for the rotational constants and quadrupole coupling strengths have been obtained for asymmetric top acyl methyl manganese pentacarbonyl from the earlier high-resolution spectroscopic measurements. These results provide a quantum mechanical-level insight into the structural properties and electric charge distribution, which are essential for understanding electronic structures of the molecule.

We have obtained a satisfactory least-squares fit analysis of the hyperfine spectrum of the dihapto isomer of acyl methyl manganese pentacarbonyl. The new

results have yielded nuclear quadrupole coupling constants that are in good agreement with the current quantum chemical calculations comparing with the previous results. The low root mean square deviation of the fit gives us confidence that the new assignments are correct. We believed the new values of nuclear quadrupole coupling constants to be more accurate than values reported previously. Given that we had a limited number of rotational transitions to work with and complications from overlapping and broadening of hyperfine lines, we view the current least squares fit results with some caution. For this asymmetric top case, the quantum number assignments of ⁵⁵Mn hyperfine components were not as straightforward as several factors complicated the analysis. One factor was that the hyperfine components fell in the spectral region with somewhat heavy spectral congestion. Some possible origins of the congestion are a) methyl internal rotation splitting and b) the presence of lines from the agostic isomer. The assignment of hyperfine lines was further complicated by the following facts: both a-type and c-type hyperfine splitting patterns show asymmetrical splitting patterns with respect to the central frequency; there appears, in some cases, additional partially resolved splitting on top of the hyperfine components; and that a-type transitions have relatively small asymmetry splitting smaller than the hyperfine splittings. A consequence of this complication is that the strong hyperfine components, especially of the a-type transitions, are clustered about the hypothetical central frequencies with few outlier satellite components. Though we were able to pick out and assign a good number of lines from the cluster, several outlier satellite components that lie away from the clusters were not observed and therefore were not included in the current hyperfine least squares fit analysis. As seen in Figure 2 and Table 2, a cluster of lines about 6435 MHz for $J = 3 \rightarrow 4$ and $4 \rightarrow 5$, $\Delta F = 0$, ± 1 transitions fit relatively well, but the current fit is missing several outlier satellite hyperfine components. Because the spread of hyperfine structure determines the magnitude of the nuclear quadrupole coupling constants, including these outlier satellite components in the least squares fit analysis would make the assignment more concrete and yield more precise values of the nuclear quadrupole coupling constants.

The diagonal components of the nuclear quadrupole coupling tensor in the principal axis for the asymmetric top acyl methylmanganese pentacarbonyl obtained

from the new least-squares fit analysis are in good agreement qualitatively with the calculated values shown in Table 3. The measured diagonal components in the principal axis are eQq_{aa} = -31.31(7), eQq_{bb} = 42.52(12), and eQq_{cc} = -11.23(12) MHz. Also, the sign of the eQq(55 Mn) obtained from this work agrees with calculated eQq(55 Mn) values computed at various level of calculations as displayed in Table 3. In the previous work, the magnitude of eQq(55 Mn) was determined correctly but not the sign as seen in Table 1 partly due to the differences in the quantum number assignments and fewer lines used in the fit. The centrifugal distortion constants D_J and D_{JK} also were obtained from the new least-squares analysis, providing for the first time some perspective into the rigidity of metal-ligand bonds in this complex. The centrifugal distortion constants, D_J = 0.21(2) and D_{JK} = 4.9(2) kHz, obtained from the least squares fit are relatively small in value. We can infer that the gas-phase structure of this molecule in the ground vibrational state has a fairly rigid structure.

It is insightful to compare the nuclear quadrupole coupling constants of CH₃(CO)Mn(CO)₄ to that of CH₃Mn(CO)₅ and HMn(CO)₅. The measured eQg(⁵⁵Mn) values along the principal symmetry axis for CH₃(CO)Mn(CO)₄, CH₃Mn(CO)₅, and $HMn(CO)_5$ are $eQq_{aa} = -31.31(7)$, $eQq_{cc} = -87.37(23)$, and $eQq_{cc} = -44.22(1)$ MHz respectively. From these eQq(55Mn) data, we can make inference about the electric field gradient distribution along the symmetry axis of the molecule (assuming eQqabc coincides with eQq_{xyz}). The electric field gradient coupling constant (q) along the symmetry axis has a negative sign for all of these transition metal complexes. However, as we can see, the asymmetric top CH₃(CO)Mn(CO)₄ has smaller negative value of eQq_{aa} = -31.31(7) MHz, approximately two and three times smaller than that of symmetric top CH₃Mn(CO)₅ and HMn(CO)₅ respectively. In comparison with HMn(CO)₅, we can explain that the decrease is due to bond lengthening. We would like to first emphasize the nature of metal-ligand coordination. In HMn(CO)₅ and CH₃Mn(CO)₅, the H-Mn and CH₃-Mn bonds are strictly sigma bond where as in CH₃(CO)Mn(CO)₄ it is dihaptic η^2 -coordination. The calculated η^2 -CH₃(CO)-Mn \cong 2.0 Å bond length is significantly longer than the H-Mn \cong 1.6 Å bond lengths. The longer η^2 -CH₃(CO)-Mn bond in CH₃(CO)Mn(CO)₄ could be invoked to explain the smaller q coupling constant; this is because the electric field potential depends on inverse of the cube of distance

 $(1/r^3)$. On the other hand, the CH₃-Mn \cong 2.0 Å bond length in CH₃Mn(CO)₅ is about the same as the η^2 -CH₃(CO)-Mn bond length surprisingly, so in this case bond lengthening argument cannot adequately explain the decrease. The different eQq(55 Mn) values tell us that the electron charge density distribution is distributed differently along the principal symmetry axis. Because manganese d-electrons are essentially nonbonding and the same configuration in these complexes, a major contribution to electron charge density distribution distortion would be the differences in the mixing of valence s and p orbitals between the metal and the six ligands. The smaller eQq_{aa} = -31.31(7) MHz value suggested that overall the electron charge density distribution along the η^2 -CH₃(CO)-Mn bond is more symmetrical than that of CH₃Mn(CO)₅ and HMn(CO)₅. This result is counterintuitive. Intuitively, one would think that a molecule with higher symmetry would have a more symmetrical charge distribution, but this is not what we see in these transition metal carbonyl complexes.

The present microwave work has improved the value of rotational constants and the diagonal elements of the nuclear quadrupole coupling tensor for the asymmetric top acyl methyl manganese pentacarbonyl. Now, for the dihapto acyl isomer calculated values for both rotational constants and quadrupole coupling strengths agree well with the measurements. For the symmetric top isomer, the calculated quadrupole coupling constants (eQqcc) had a large variance and are poor agreement with the experimentally determined eQqcc. Microwave measurements of the nuclear quadrupole coupling constants and rotational constants are of considerable importance because these spectroscopic constants provide a touchstone to test the reliability and accuracy of computational methods.

Acknowledgements

This material is based upon work supported by the National Science Foundation under Grant No. CHE-1057796 at the University of Arizona. CAJH is grateful for support from a start-up package from Wesleyan University. We are very grateful to UITS-HPC computing facilities for the computing time provided on the Ocelote system.

This material is based, in part, upon High Performance Computing (HPC) resources supported by the University of Arizona TRIF, UITS, and Research, Innovation, and Impact (RII) and maintained by the UArizona Research Technologies department. We thank Jimmy Ferng for assistance with the calculations, which was made possible through University of Arizona Research Technologies Collaborative Support program.

https://public.confluence.arizona.edu/display/UAHPC/Compute+Resources

^{1.} Calderazzo, F.; Cotton, F.A. Carbon Monoxide Insertion Reactions. I. the Carbonylation of Methyl Manganese Pentacarbonyl and Decarbonylation of Acetyl Manganese Pentacarbonyl. *Inorganic Chemistry*, **1962**, 1, 30-36.

^{2.} Noack, K.; Calderazzo, F. Carbon Monoxide Insertion Reactions V. The Carbonylation of Methylmanganese Pentacarbonyl with 13CO *Journal of Organometallic Chemistry*, **1967**, 10, 101-104. https://doi.org/10.1016/S0022-328X(00)81721-0

^{3.} Noack, K.; Ruch, M.; Calderazzo, F. Carbon Monoxide Insertion Reaction. VI. The Mechanisms of the Reactions of Methylmanganese Pentacarbonyl and Acetylmanganese Pentacarbonyl with Triphenylphosphine. *Inorganic Chemistry*, **1968**, 7, 345-349.

^{4.} Derecskei-Kovacs, A.; Marynick, D.S. A New Look at an Old Reaction: The Potential Energy Surface for the Thermal Carbonylation of Mn(CO)₅CH₃. The Role of Two Energetically Competitive Intermediates on the Photodecarbonylation of Mn(CO)₅(COCH₃). *J. Am. Chem. Soc.* **2000**, 122, 2078-2086. https://doi.org/10.1021/ja993441v

^{5.} C. Tanjaroon, Z. Zhou, D. Mills, K. Keck, and S. G. Kukolich, Inorg. Chem. 59 (2020), 6432 – 6438

^{6.} T. J. Balle and W. H. Flygare, Rev. Sci. Instrum., 52(1981), 33.

^{7.} H.M.J. Pickett, J. Mol. Spec., 148 (1991), 371.

^{8.} V. Kellö, A. J. Sadlej, P. Pyykkö, Chemical Physics Letters, 329(2000), 112-118

^{9.} P. P. Pyykkö, Molecular Physics, 99(2001), 1617-1629

^{10.} Arizona High-Performance computing resources.

^{11.} Frisch, M. J.; Trucks, G. W.; Schlegel, H. B.; Scuseria, G. E.; Robb, M. A.; Cheeseman, J. R.; Scalmani, G.; Barone, V.; Petersson, G. A.; Nakatsuji, H.; Li, X.; Caricato, M.; Marenich, A.; Bloino, J.; Janesko, B. G.; Gomperts, R.; Mennucci, B.; Hratchian, H. P.; Ortiz, J. V.; Izmaylov, A. F.; Sonnenberg, J. L.; Williams-Young, D.; Ding, F.; Lipparini, F.; Egidi, F.; Goings, J.; Peng, B.; Petrone, A.; Henderson, T.; Ranasinghe, D.; Zakrzewski, V. G.; Gao, J.; Rega, N.; Zheng, G.; Liang, W.; Hada, M.; Ehara, M.; Toyota, K.; Fukuda, R.; Hasegawa, J.; Ishida, M.; Nakajima, T.; Honda, Y.; Kitao, O.; Nakai, H.; Vreven, T.; Throssell, K.; Montgomery, J. A., Jr.; Peralta, J. E.; Ogliaro, F.; Bearpark, M.; Heyd, J. J.; Brothers, E.; Kudin, K. N.; Staroverov, V. N.; Keith, T.; Kobayashi, R.; Normand, J.; Raghavachari, K.; Rendell, A.; Burant, J. C.; Iyengar, S. S.; Tomasi, J.; Cossi, M.; Millam, J. M.;

Klene, M.; Adamo, C.; Cammi, R.; Ochterski, J. W.; Martin, R. L.; Morokuma, K.; Farkas, O.; Foresman, J. B.; Fox, D. J. Gaussian 09, Revision A.1; Gaussian, Inc., Wallingford CT, 2016.